The Effect of Additives on Amorphous Calcium Carbonate (ACC): Janus Behavior in Solution and the Solid State

*Johannes Ihli, Yi-Yeoun Kim, Elizabeth H. Noel, and Fiona C. Meldrum**

Amorphous calcium carbonate (ACC) is an important intermediate in the formation of crystalline $CaCO_3$ biominerals, where its crystallization is controlled using soluble additives. However, although this transformation often occurs in the solid state, experiments mainly focus on the effect of additives on ACC crystallization in solution. This paper addresses this issue and compares the crystallization, in solution and in the solid state, of ACC precipitated in the presence of a range of additives. Surprisingly, these results show that some additives exhibit a Janus behavior, where they retard crystallization in solution, yet accelerate it in the solid state. This is observed for all of the larger molecules examined, while the small molecules retard crystallization in both solution and the solid state.

1. Introduction

Biominerals, with their remarkable morphologies and properties, demonstrate that it is possible to achieve remarkable control over crystallization processes under ambient reaction conditions.[1] Study and characterization of the strategies employed by nature has then enabled translation of many of these principles to synthetic systems.[2] Of the biological strategies identified, the most versatile is arguably the use of soluble additives. The role of soluble additives in controlling crystallization has been particularly well-studied for the calcium carbonate system, where organic macromolecules have been extracted from within biominerals and crystals then precipitated de novo from solution in their presence. This approach has demonstrated that these macromolecules can bind selectively to certain families of crystal faces, modifying morphologies, crystal textures, and mechanical properties.[3] In combination with insoluble organic matrices, certain bio-macromolecules also appear to offer control over crystal polymorphs.[4]

While these studies have yielded valuable information on the interaction between bio-macromolecules and calcium carbonate crystals, the finding that many biominerals form via amorphous precursor phases rather than ion-by-ion growth,[5,6] raises questions concerning the mechanisms by which additives participate in the crystallization of the amorphous phase. Looking specifically at amorphous calcium carbonate (ACC), while this phase is typically very short-lived when precipitated in the absence of additives, it can be stable indefinitely as a biomineral. As a transient precursor phase, ACC can also undergo controlled transformation to either calcite or aragonite, via a stepwise transition from hydrated ACC, to anhydrous ACC, to the final crystal polymorph.[7,8] The extended stability of biogenic ACC, and the ability of organisms to be able to control the nucleation and crystallization of this phase, has been attributed to organic and inorganic additives present within the mineral phase, where high levels of magnesium, phosphate, and glycoproteins rich in glutamic acid and hydroxyamino acids (which are potentially phosphorylated) are characteristic.[9] The small molecules phosphoenolpyruvate and 3-phosphoglycerate, which are intermediates of the glycolic pathway, have also been found to be important in stabilizing ACC in the exoskeleton and gastroliths of crustaceans.[10] Taking inspiration from this strategy, highly carboxylated species including poly(acrylic acid),[11] a poly(ethylene oxide)-*block*-poly(acrylic acid) block copolymer,[12] and poly(aspartic acid)[7,13] have been widely used to extend the lifetime of synthetic ACC in solution, as have magnesium[14,15] and phosphate ions.[16] Other effective species have included poly(allylamine hydrochloride) (PAH),[17] poly(styrene sulphonate),[11] ovalbumin,[18] and silicate.[19]

While research has focused on the effects of additives on ACC in solution, it is notable that crystallization of ACC may well occur via a solid-state transformation in biology. Looking at the best-studied system – that of the sea urchin larval spicule – the ACC precursor phase is encapsulated within a membrane-bound compartment, such that it is effectively crystallizes in the absence of bulk water.[20] Crystallization then proceeds without an identifiable crystallization front, possibly by secondary nucleation among ACC nanoparticles.[21] That the absence of bulk water may play a key role in extending the lifetime of the ACC is also supported by the observations that synthetic ACC crystallizes significantly more slowly when dry than in solution, or when it has only limited contact with water.[22–24] Further, precipitation of $CaCO_3$ from alcohol containing little or no water also yields ACC which can be stable for long periods, particularly when species such as magnesium ions are additionally present.[25]

Given the importance of a solid-state crystallization mechanism to the transformation of ACC to crystalline $CaCO_3$ biominerals, it is then perhaps surprising that the ability of additives to direct this process has received such little attention.[11] Indeed, the crystallization of dry ACC (i.e., in the solid state)

J. Ihli, Dr. Y.-Y. Kim, E. H. Noel, Prof. F. Meldrum
School of Chemistry, University of Leeds
Woodhouse Lane, Leeds, LS2 9JT, UK
E-mail: F.Meldrum@leeds.ac.uk

DOI: 10.1002/adfm.201201805

has primarily been studied during differential scanning calorimetry (DSC), which is not ideally suited to monitoring slow transitions. In this article, we address this issue, and compare the crystallization of a range of amorphous calcium carbonate samples, which were precipitated in the presence of different additives, in solution and in the solid state. Our data reveal a surprising phenomenon, in that some additives exhibit a contrasting, Janus like behavior, where they show the anticipated ability to retard crystallization of ACC in solution, but yet accelerate a solid-state crystallization. Interpretation of this result is made by considering whether the action of the additives is direct, by altering the stability of the ACC, or indirect, by suppressing/retarding formation of the emerging crystalline polymorph.

2. Results

The influence of the additives magnesium, sulfate, aspartic acid (Asp), poly(styrene sulphonate) (PSS), poly(aspartic acid) (PAsp), and bis(2-ethylhexyl)sulfosuccinate (AOT) associated with innocent spectator ions (Cl^- and Na^+) on the crystallization of amorphous calcium carbonate (ACC) in both solution and in the solid state was evaluated and compared. Their behavior in solution was investigated by using turbidity measurements to monitor the crystallization of ACC precipitated in the presence and absence of additives, and by determining the dissolution profiles of different pre-prepared ACC samples. Solid-state crystallization, in contrast, was studied by annealing dried ACC powders, through DSC, and by performing in situ powder X-ray diffraction (XRD) analysis while heating dry ACC precipitates.

The majority of experiments were carried out with ACC which was synthesized by mixing equal volumes of solutions of 1 M Na_2CO_3/30 mM NaOH and 1 M $CaCl_2$ at 4 °C, although a number of other methods were also employed, as described in the text. All of the types of ACC samples were characterized using IR spectroscopy and Raman microscopy, powder XRD, X-ray absorption spectroscopy (XAS) and scanning electron microscopy (SEM) or transmission electron microscopy (TEM) to confirm their amorphous character. Typical data is shown in **Figure 1** for the ACC obtained. IR spectroscopy yielded spectra characteristic of ACC (Figure 1A and Supporting Information, Figure S1) where broad peaks centered around 1476/1414 cm^{-1} (ν_3), 1075 cm^{-1} (ν_1) and 865 cm^{-1} (ν_2) are observed, in addition to peaks due to the vibration of water molecules at 1651 cm^{-1}.[26] Raman spectroscopy, in turn, showed a very broad peak at 1085 cm^{-1}, corresponding to the internal CO_3^{2-} symmetric stretch, and a notable absence of the ν_4 peak around 700 cm^{-1} (Figure 1B).[27] Powder XRD (Supporting Information, Figure S2) and electron diffraction (Figure 1D, inset) confirmed this analysis through the complete absence of any sharp peaks, and the presence of an initial, broad amorphous background/rings. The pre-edge and X-ray absorption near edge structure (XANES) regions of the Ca-edge XAS spectra of the pure ACC were typical of ACC reported in the literature, showing a single large peak at the top of the absorption edges at 4051.28 eV, and

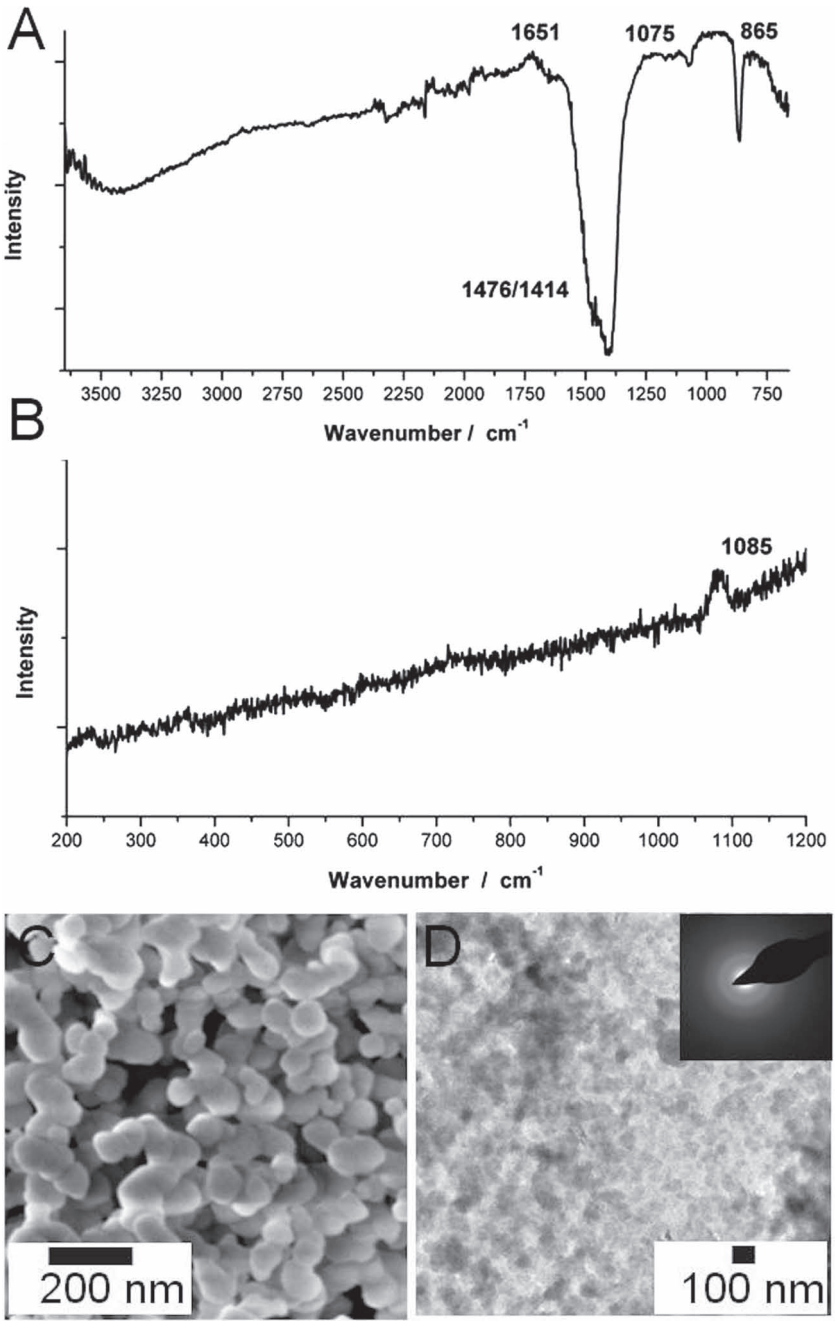

Figure 1. Characterization of pure ACC using: a) IR spectroscopy, b) Raman microscopy, c) SEM, and d) TEM, where the inset shows the corresponding electron diffraction pattern.

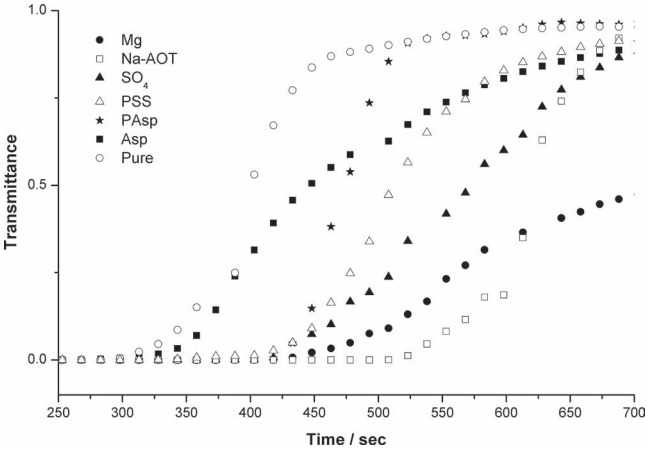

Figure 2. Progress of UV–vis transmittance recovery as a function of time after mixing two solutions of 1 M $CaCl_2$ and 1 M Na_2CO_3 containing 200 ppm of the additives, poly(styrene sulphonate) (PSS), aspartic acid (Asp), poly(aspartic acid) (PAsp), bis(2-ethylhexyl)sulfosuccinate (AOT), 10 mM of Mg^{2+}, or 2 mM SO_4^{2-}.

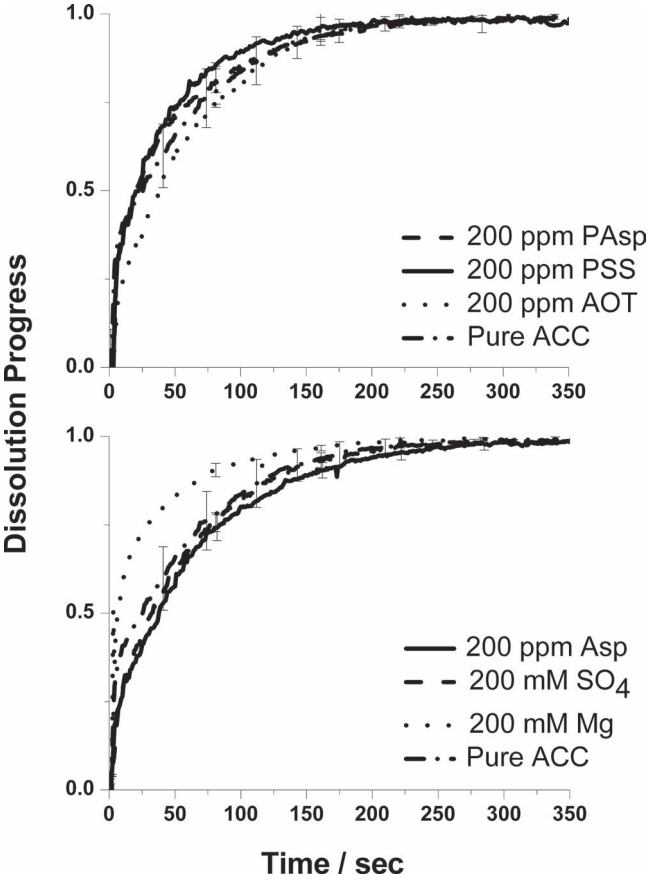

Figure 3. Dissolution behavior of ACC samples precipitated in the presence of different types and amounts of additives: Mg^{2+}, SO_4^{2-}, aspartic acid (Asp), poly(aspartic acid) (PAsp), poly(styrene sulphonate) (PSS), and bis(2-ethylhexyl)sulfosuccinate (AOT).

a pre-edge peak at 4041.47 eV, which has been attributed to 1s–3d type transitions (Supporting Information, Figure S3).[28] This contrasts with the crystalline polymorphs of $CaCO_3$ which show a number of features at the absorption edge. Similar spectra were obtained for ACC precipitated in the presence of Mg^{2+} and PAsp (Supporting Information, Figure S3). Finally, SEM and TEM demonstrated that the particles were approximately 50–80 nm in diameter (Figure 1C,D).

The influence of additives on the crystallization of ACC in solution was investigated by recording the change in the solution turbidity with time using UV–vis spectroscopy, when ACC was precipitated in the presence and absence of additives. This has been shown to provide an effective method for monitoring the early stages of precipitation of calcium carbonate in solution, when the recorded changes in light transmission with time can be related to the precipitation and aggregation of ACC, its subsequent crystallization and the gravitational sedimentation of the growing crystals.[29] It is stressed that the goal of these experiments was simply to determine whether the additives used accelerate or decelerate the rate of crystallization of the ACC, rather than to extract kinetic parameters. **Figure 2** shows graphs of the changes in the percentage transmitted light intensity as a function of time in the absence and in the presence of additives. Immediate precipitation of ACC was observed in all of the experiments, due to the high reagent concentrations employed, such that 0% transmittance was recorded at the outset of the experiments. All of the additives investigated retarded the onset of transmission recovery, which is associated with the dissolution and aggregation of ACC and the subsequent settlement of product vaterite or calcite crystals.[29] Ex situ IR measurements carried out on selected ACC samples at different time-points on the turbidity curves confirmed this analysis, showing the transformation of ACC to calcite and vaterite as the transmittance recovers (Supporting Information, Figure S4B). These measurements further confirmed that the additives investigated retarded the crystallization of the ACC phase (as shown for PSS and Mg^{2+} in Figure S4C in the Supporting Information).

Pure ACC samples showed a measured "induction time" of ≈300 s, while crystallization onsets between 320 and 500 s were recorded for ACC occluding the additives investigated, where the retardation effect was in the order AOT > PSS > PAsp > Asp for 200 ppm additives, and the conditions used in these experiments. The curves shown for Mg and SO_4 correspond to concentrations of 10 mM Mg^{2+} and 2 mM SO_4^{2-}; when the 200 mM concentrations used in many parts of this study were employed in the scattering experiments, Mg-ACC failed to crystallize within 1 day, and $CaSO_4$ co-precipitated with the ACC.

In bulk solution, the crystallization of ACC is usually accompanied by a dissolution-reprecipitation process.[16,30–33] To gain insight into whether the additives affect this process by directly influencing the stability of the ACC in solution, or via an indirect effect, where they retard the formation of the crystalline transformation product, the dissolution profiles of the different ACC samples were measured and compared. The time-resolved, normalized dissolution curves for ACC samples precipitated with and without additives are presented in **Figure 3**. These data clearly show that only very slight differences in the dissolution behavior of ACC were recorded in the presence

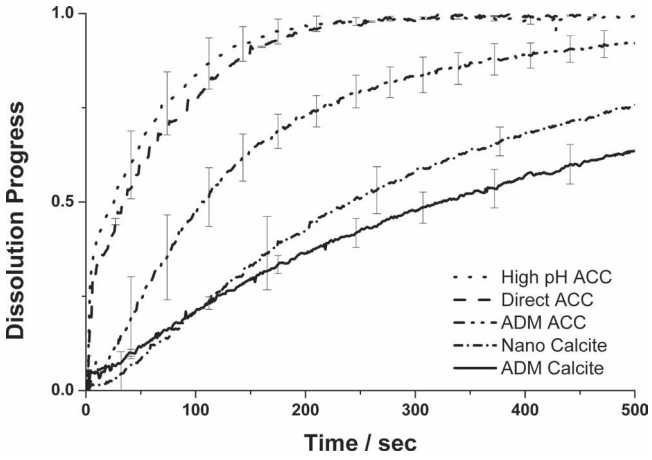

Figure 4. Dissolution behavior of calcium carbonate samples precipitated using different precipitation methods: calcite precipitated using the ammonia diffusion method (ADM Calcite), ACC precipitated by direct precipitation (Direct ACC), ACC precipitated at high pH ("high pH" ACC), ACC precipitated using the ammonia diffusion method (ADM ACC), and commercial nanosized calcite (Nano Calcite).

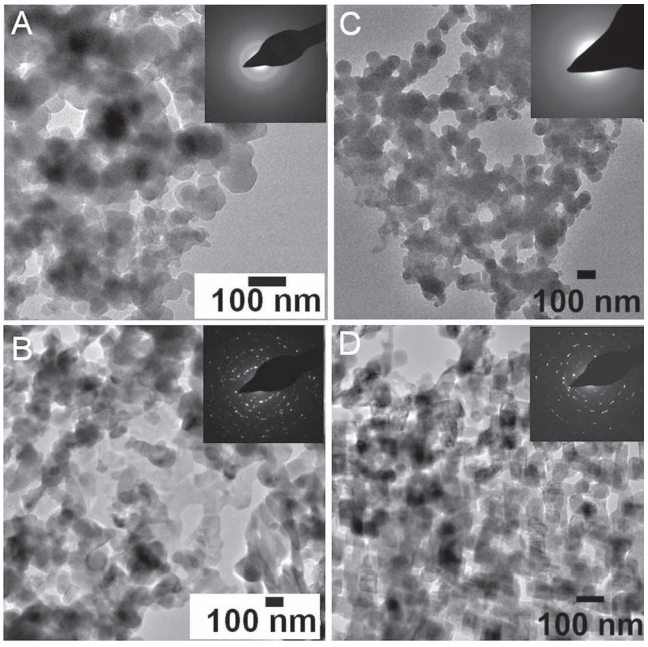

Figure 5. TEM images of: A) pure ACC after heating at 10 °C min^{-1} to 70 °C followed by 12 h incubation showing no crystallization; B) pure ACC after heating at 10 °C min^{-1} to 350 °C followed by 3 h incubation, showing crystallization; C) ACC precipitated in the presence of 200 ppm PSS; and D) PSS-ACC after heating at 10 °C min^{-1} to 70 °C followed by 12 h incubation, showing crystallization.

of the additives. Indeed, the additives primarily affected the initial rate of dissolution of the ACC, and complete dissolution of all samples was achieved after ≈300 s. The one additive that appeared to have a notable effect was magnesium, which showed a tendency to increase the dissolution rate of ACC. This result is commensurate with the higher solubility of Mg-calcite as compared with pure calcite.[34]

For completeness, the dissolution behavior of ACC prepared by a number of different methods was also investigated and compared with nano- and micrometer-sized calcite crystals. ACC was precipitated by a direct precipitation route (direct ACC – combining 1 M $NaCO_3$ with 1 M $CaCl_2$), at high pH ("high pH" ACC – combining 1M $NaCO_3$/30 mM NaOH with 1 M $CaCl_2$) and using the ammonia diffusion method, while the commercial nanocalcite was ≈100 nm in size and calcite precipitated using the ammonia diffusion method was 10 μm in size. The dissolution curves are shown in **Figure 4**, and clearly demonstrate changes in the dissolution behavior according to the synthesis method of the ACC and the size of the calcite. As anticipated, the nanocalcite dissolved faster than the micrometer-scale crystals. Interestingly, however, the ACC precipitated using the ammonia diffusion method dissolved significantly more slowly than that precipitated using any of the other methods (which were very similar). While the ammonia-diffusion-method ACC was approaching full dissolution after ≈700 s, all of the other ACC samples had achieved this level of dissolution after ≈300 s. These data confirm that amorphous calcium carbonate (as defined as $CaCO_3$ which does not diffract X-rays) is best described as a family of phases, and that direct comparison of the behavior of ACC prepared by different methods should be made with caution.

The influence of additives on the crystallization of ACC was also investigated in the solid state. This was again evaluated using a number of different approaches, including annealing samples at moderate temperatures, through thermal analysis, and by performing in situ powder XRD analysis in air while heating the ACC precipitates. Examination of the ACC after annealing at 70 °C for 12 h showed that it did not crystallize under these conditions (**Figure 5**A and Supporting Information, Figure S1A). The same behavior was observed for ACC precipitated in the presence of 200 mM Mg^{2+} and SO_4^{2-} and 200 ppm Asp. In contrast, ACC samples precipitated in the presence of 200 ppm AOT, PSS, and PAsp all crystallized under the same heating regime. This was demonstrated using electron diffraction (Figure 5B) and also IR spectroscopy, where the product particles showed peaks at 875 $cm^{-1}(\nu_2)$ and 713 $cm^{-1}(\nu_4)$, confirming the formation of crystalline precipitates,[26] (representative data for PSS and AOT is shown in Figure S1 in the Supporting Information). Notably, TEM examination of the ACC particles before and after heating revealed that while the pure ACC particles sintered together somewhat on heating to 70 °C and after crystallization at 350 °C, there was little change in the original spherical form of the particles (Figure 5B,C). The additive-ACC particles, in contrast, transformed to partially sintered rhombohedral calcite particles on annealing at 70 °C (Figure 5D shows PSS-ACC after crystallization).

The role of water loss on ACC crystallization at 70 °C was also investigated by performing simultaneous thermogravimetric analysis and differential scanning calorimetry (TGA-DSC) under isothermal conditions at 70 °C (>12 h) for additive-free ACC and PSS-ACC. Both samples revealed an initial weight loss of ≈4–6 wt%, identifiable as physisorbed water. This was followed by a gradual loss of structural water upon isothermal storage, corresponding to 17 wt% in total or ≈85% of all structural water (based on a molar composition of 1 $CaCO_3$:1 H_2O)

Table 1. Activation energies, peak temperatures, and the percentage of water present with ACC samples precipitated in the presence and absence of the additives Mg^{2+}, SO_4^{2-}, aspartic acid (Asp), poly(aspartic acid) (PAsp), poly(styrene sulphonate) (PSS), and bis(2-ethylhexyl)sulfosuccinate (AOT), as obtained by DSC and TGA. All of the data presented represent average values.

	Additives						Pure ACC
	Group 1 $M_w < 400$ g mol^{-1}			Group 2 $M_w > 400$ g mol^{-1}			
	Mg	SO_4	Asp	AOT	PAsp	PSS	
Additive Conc.[a] [mM]	200	200	1.5	0.5	1.5	0.9	–
Wt% Additives	6	3	1.5	0.9	1.4	1.7	–
Wt% H_2O	23.6	20.7	19.4	20.5	19.4	21.3	20.2
10 °C min^{-1} T_P [°C]	332.66	330.49	328.66	325.98	324.86	323.57	328.10
15 °C min^{-1} T_P [°C]	344.63	339.49	336.97	332.85	331.02	329.39	335.63
25 °C min^{-1} T_P [°C]	351.22	342.67	339.27	334.80	334.83	332.26	337.48
Approximate E_A [kJ mol^{-1}]	351	291	271	228	207	206	246

[a]Additive concentrations with respect to the number of functional groups.

(Supporting Information, Figure S5). Loss of this water seemingly allowed the crystallization of PSS-ACC samples at 70 °C, while the pure ACC samples only crystallized at temperatures over 335 °C. This was well after the remaining structural water had been lost at ≈200 °C. This apparent critical temperature of ≈330 °C was also confirmed by preheating pure ACC for 12 h at 230 °C prior to further increasing the temperature to initiate crystallization in order to to exclude kinetic effects.

ACC samples occluding additives were also analyzed using continuous TGA and DSC to compare the effects that the different additives have on the apparent crystallization temperature. Typical TGA and DSC profiles for pure ACC are shown in Figure S6 in the Supporting Information, and a summary of results is presented in **Table 1**. Identical amounts of samples (≈10 mg) were used in all the runs, and heating rates of 10 °C min^{-1}, 15 °C min^{-1}, and 25 °C min^{-1} were applied. TGA and atomic adsorption (AA) demonstrated that small quantities (≈ 1–2 wt%) of the organic additives Asp, PAsp, PSS, and AOT were associated with ACC, while approximately 3 wt% and 6 wt% of the inorganic additives SO_4^{2-} and Mg^{2+} were present, respectively. TGA further revealed no significant difference in the total amount of water associated with the ACC samples, with values ranging between 19.4 and 21.3 wt% H_2O. Mg-ACC contained the somewhat higher amount of 23.6 wt% H_2O (Table 1 and Supporting Information, Figure S6).

Figure 6 shows typical DSC curves (recorded at a heating rate of 15 °C min^{-1}) for ACC samples precipitated in the absence and presence of additives, in the region of the exothermic transition from ACC to calcite. This Figure clearly shows that the additives affect both the crystallization temperature and the peak shape. Crystallization peak temperatures (T_P) between 326 °C and 344 °C were recorded for ACC precipitated in the presence of 200 ppm (<2 mM) of the organic additives or 200 mM of the inorganic ions. The most-significant increase in crystallization temperature occurred with magnesium ions, while PSS lowered the crystallization temperature the most. In making this statement, however, we emphasize that the concentrations of the additives employed necessarily affect the magnitude of their effect on the crystallization temperature, but not the direction of the temperature change.

Based on the inherent differences in the solubilities of the organic and inorganic additives, and the differences in additive concentrations employed, on a mole-per-mole basis (considered with respect to the functional groups on the polymer) the polymers have much larger effects on ACC crystallization than the inorganic ions. Given the recorded ACC crystallization temperatures of ≈320–350 °C (Table 1), possible decomposition of the additives used also has to be considered. Analysis of the TGA curves obtained for both pure ACC, and ACC containing additives, (Supporting Information, Figure S6A) showed that there was no detectable weight loss associated with decomposition of the organic additives. TGA analysis of the pure additives was also performed under nitrogen (Supporting Information, Figure S8) to provide a clearer picture of their thermal stabilities, and the organic additives PAsp, Asp, and AOT were observed to decompose partially at temperatures below those at which

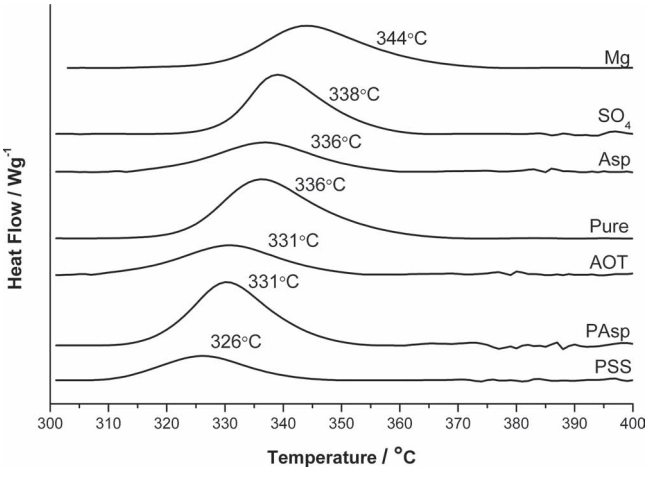

Figure 6. A sectional view of ACC samples DSC scans showing the exothermic peak corresponding to the transition from ACC to calcite. A heating rate of 15 °C min^{-1} was applied. ACC samples were precipitated in the presence of selected additives Mg^{2+}, SO_4^{2-}, aspartic acid (Asp), poly(aspartic acid) (PAsp), poly(styrene sulphonate) (PSS), poly(aspartic acid) (PAsp), and bis(2-ethylhexyl)sulfosuccinate (AOT).

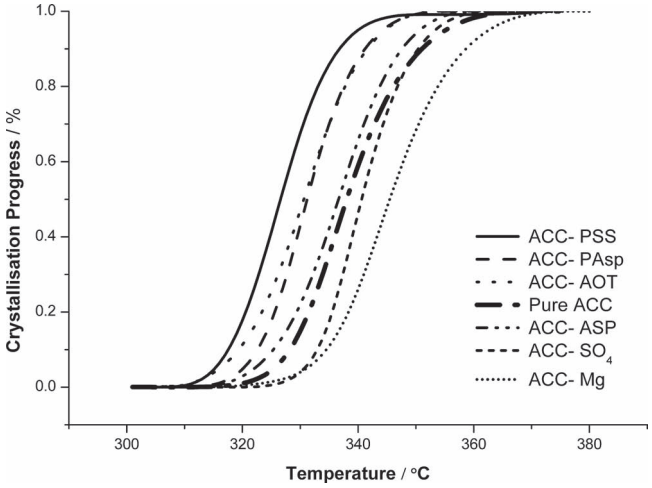

Figure 7. Crystallization progress of ACC samples precipitated in the presence of Mg^{2+}, SO_4^{2-}, aspartic acid (Asp), poly(aspartic acid) (PAsp), poly(styrene sulphonate) (PSS), and bis(2-ethylhexyl)sulfosuccinate (AOT), as derived from DSC scans performed with a heating rate of 15 °C min^{-1}. The time axis shows the time required to complete crystallization after the first change in heat flow associated with crystallization ($t = 0$) was detected.

crystallization of the ACC occurred. Asp decomposed most readily, starting around ≈230 °C, while PSS was stable until 380 °C. ACC containing sulfate showed no significant structural decomposition before crystallization, whereas Mg-ACC showed a significant weight loss associated with water loss immediately before crystallization (Supporting Information, Figure S6, S8).

The crystallization temperatures measured are consistent with those reported for DSC analysis of pure ACC in the literature, where crystallization temperatures of 320–350 °C have generally been recorded.[35–37] Notably, the pH at which the ACC is precipitated has been reported to affect the crystallization temperature, with a value as low as ≈ 210 °C having been measured for ACC precipitated at pH 11.2,[36] and a crystallization temperature of 277 °C being given for ACC precipitated from a dimethyl carbonate solution.[38] Addition of silicate to ACC was reported to result in a remarkable increase in the crystallization temperature to 384 °C.[19] This range in recorded temperatures serves to emphasize that it is nonsense to quote a definite value for the crystallization temperature of "ACC". The temperature measured depends on a wide range of variables, including the methods used to synthesize and isolate the ACC from solution.

As a most-striking result, it is possible to classify the additives used into two distinct groups: those which increase the crystallization temperature (Mg^{2+}, SO_4^{2-}, and, to a lesser, extent Asp) as compared with pure ACC, and those which lower it (AOT, PSS, and PAsp). Examination of the molecules belonging to each group therefore shows that the high-molecular-weight additives lower the apparent crystallization temperature, whereas the smaller additives exhibit the reverse behavior. The DSC measurements were also used to derive curves of the crystallization progress, assuming Johnson–Mehl–Avrami transformation behavior (**Figure 7**).[39] The trends in the data were largely in keeping with the recorded crystallization temperatures, such that the curve for the Mg-ACC sample appeared at the highest temperature and the PSS-ACC sample the lowest. The curves for the ACC precipitated with the three high-molecular-weight additives were shifted to lower temperatures as compared with the ACC associated with the low molecular weight additives.

It was also possible to derive a number of thermodynamic quantities from the DSC and TGA data. Estimation of the enthalpies of crystallization (ΔH_{cryst}) of the different ACC samples was made from the areas of the crystallization peaks, based on the quantity of anhydrous ACC present, as determined from the corresponding TGA profiles.[35] All except the Mg-ACC fell within the range −18 to −31 kJ mol^{-1} where the errors in the data were such that no statistical difference was recorded as compared with the value of $\Delta H_{cryst} = -21.93 \pm 6.13$ kJ mol^{-1} for the control sample. The Mg-ACC sample, by contrast, exhibited a significantly higher $\Delta H_{cryst} = -58.59 \pm 6.44$ kJ mol^{-1}. The activation energies (E_A) associated with the transformation of anhydrous ACC to calcite were derived from DSC scans carried out at different heating rates, as calculated using the method of Ozawa.[40] The values fell within the range 207–352 kJ mol^{-1} (Table 1) and are in good agreement with those of 152–304 kJ mol^{-1} derived by Koga et al. for pure ACC precipitated at different pH values.[36] In hindsight to the pH dependence reported by Koga, it is noted that a maximum difference in starting pH of 1.5 units was recorded for the ACC samples investigated here (Supporting Information, Table S1), and that no correlation was observed between the shifts in crystallization temperature and the initial pH values.

The validity of this pattern was also confirmed by recording XRD spectra of ACC samples during in situ heat treatment in air. Rapid scans were carried out over the interval $2\theta = 28–32°$, to monitor the development of the {104} peak of calcite (where prior runs had demonstrated the absence of a vaterite intermediate phase). As noted previously, although the trends in the crystallization temperatures are maintained for all ACC samples, the particular values recorded depend strongly on the method used to synthesize the ACC and the analysis conditions. Both "high pH" ACC and ACC prepared using the 1 M $(NH_4)_2CO_3$ in the presence and the absence of selective additives (PSS, PAsp, and Mg^{2+}) were therefore studied using XRD. All ACC samples showed a broad crystallization transition, taking place over a temperature range of 150 °C, with onset temperatures of ≈220 °C and above. Similar trends were found for ACC prepared using both methods, and data for ACC using ammonium carbonate as a carbonate source is shown in **Figure 8** (with an alternative presentation given in Figure S7 in the Supporting Information). Here, the ACC precipitated in the presence of PAsp and PSS began to crystallize at lower temperatures, with slightly higher crystallization rates than pure ACC, while ACC precipitated with Mg started to crystallize at higher temperatures.

3. Discussion

Investigations of the effects of additives occluded within amorphous calcium carbonate on the crystallization of ACC in solution and in the solid state clearly show that additives can display different patterns of behavior in directing crystallization in these

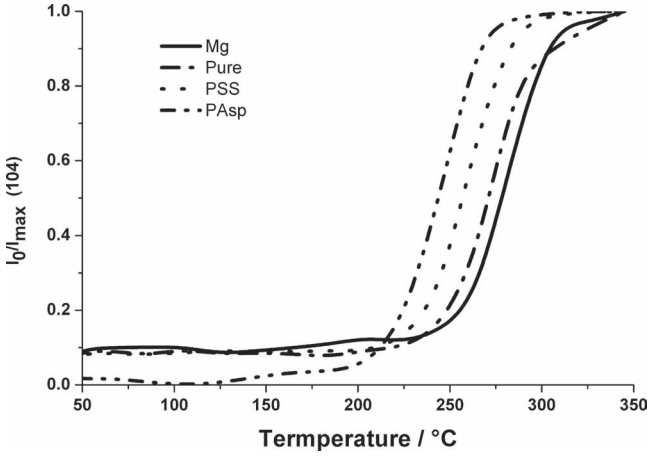

Figure 8. Crystallization-temperature profiles of ACC prepared by mixing 1 M $CaCl_2$ with 1 M $(NH_4)_2CO_3$/30 mM NaOH in the absence or presence of PAsp, PSS (200 ppm) or Mg^{2+} (200 mM), as measured using powder XRD analysis of samples heated in situ in a diffractometer. The data are expressed as the recorded intensity of the {104} peak of calcite (I_0) with respect to the maximum intensity measured after complete crystallization (I_{max}).

two contrasting environments. This provides some insight into the possible mechanisms of ACC crystallization, and, in doing so, also challenges some common ideas regarding the role of additives in stabilizing ACC. Considering first crystallization in solution, investigations of the crystallization behavior of ACC occluding additives showed that all of the additives used retarded the crystallization of the ACC in solution. Crystallization of ACC in solution takes place with nucleation and growth of the new crystal phase, which is accompanied by dissolution of the ACC. Thus, zones depleted of ACC particles have often been observed adjacent to calcite crystals growing on solid substrates from suspensions of ACC.[31,32] Simultaneous SAXS/WAXS studies of the transformation of ACC have demonstrated that the heterogeneous nucleation and growth of calcite on the walls of the reaction vessel is accompanied by dissolution of the ACC,[33] while measurement of the changes in the solution composition which occur on crystallization of ACC to vaterite and calcite also show that the solution composition (as expressed in the ion activity product) remains at the level of the least stable polymorph present.[16] The solution is therefore supersaturated with respect to calcite and vaterite during crystallization of the ACC to these phases, which demonstrates that the rate-determining step is the growth of the crystalline phases rather than dissolution of the ACC. This is also supported by our dissolution studies, which show that there was negligible change in the ACC dissolution profile when additives were occluded within the mineral.

This indicates that in solution, the additives either retard the growth of the new crystalline phase, and/or they inhibit its nucleation. No structural or compositional change occurs in the ACC which inhibits its dissolution, a process which occurs concomitantly with formation of the new crystal phase. A retardation of the growth of calcite or vaterite would certainly occur when additives, released on dissolution of the ACC, bind to nascent crystals, thereby inhibiting their growth. Indeed, it is well-documented that magnesium,[41–43] phosphate,[43,44] Asp,[45] poly(aspartic acid),[46] sulfate,[43,47] and poly(styrene sulfonate)[11] can all inhibit the growth of calcite at sufficient concentrations, where this effect can be both kinetic and thermodynamic in origin. For example, both magnesium and sulfate ions are incorporated within the calcite lattice, causing a change in lattice parameters, an increase in solubility, and a reduction in thermodynamic stability as compared with pure calcite.[15,42,48] The effect of additives on growing crystals can also be considered in terms of their interaction with step edges and kink sites, where, for example, blocking of a kink site by an additive would give rise to kinetic inhibition of growth.[49]

The influence on nucleation would depend on whether this occurs de novo from solution, or if it takes place within existing ACC particles. Whether calcite/vaterite nucleate from suspensions of ACC in solution either de novo, or within existing ACC particles, has not been conclusively proven – and is likely to vary according to the experimental conditions. Some support for nucleation within ACC particles has come from cryo-TEM studies of the crystallization of ACC particles in association with Langmuir monolayers,[50] and the observation of aggregation of ACC particles prior to crystallization to calcite on self-assembled monolayers (SAMs).[30] Whether identical behavior occurs during crystallization in solution, however, is unclear. Investigation of the size-dependent stability of ACC in solution has suggested that there is a critical size limit below which ACC is stable, which again supports a homogeneous nucleation mechanism in some circumstances.[51,52] Crystallization of ACC to vaterite in bulk solution via a solid state transformation has also been suggested, based on SAXS/WAXS studies.[53] The ACC nanoparticles were believed to first dehydrate, then undergo a structural rearrangement to vaterite, and finally aggregate to form micrometer-scale vaterite particles.

A different, and interesting, pattern of behavior was seen for the crystallization of ACC in the solid state. On annealing pure ACC samples at moderate temperatures (70 °C) for 12 h, no crystallization was observed. In contrast, ACC co-precipitated with 200 ppm AOT, PSS, and PAsp crystallized under the same conditions. These additives therefore effectively promote crystallization of ACC in the solid state, while inhibiting it in solution. These samples were also analyzed under much higher heating rates using DSC-TGA, which confirmed that the additives could be divided into two distinct groups based on their action, where the low-molecular-weight compounds (Mg^{2+}, Asp, and SO_4^{2-}) stabilized the ACC against crystallization in the solid state, while the high-molecular-weight compounds (AOT, PSS, and PAsp) promoted it.

Although the TGA results show the same pattern of behavior as the low-temperature isothermal crystallizations, it is stressed that all of the organic additives (with the notable exception of PSS, which was the most effective additive in lowering the ACC crystallization temperature) are likely to have undergone partial decomposition prior to ACC crystallization at the temperatures encountered for ACC crystallization in the TGA measurements. That the additives still affect ACC crystallization even after partial decomposition, to the extent that the small and larger additives increase and reduce the crystallization temperature, respectively, is intriguing. Indeed, this suggests that the

additives may affect the structure of the ACC phase at the point of formation, which in turn dictates its subsequent ease of crystallization in the solid state. The presence of water, and how it is located within ACC is also expected to affect the crystallization of this phase. However, all of the ACC samples investigated here were analyzed for both surface-bound and structural water and little variation between samples was observed.

Our data therefore suggest that additives with small and large molecular weights may affect ACC crystallization by different mechanisms. Assuming that the additives are mixed with the ACC at a molecular level, the large additives may increase the free volume present in the ACC, enhancing the molecular mobility and reducing the activation barrier to crystallization. This argument is consistent with the reduced activation energies derived from the DSC analyses. It is also possible that the large additives reduce the entropic penalty for crystallization.[54] Functional groups in the additives may induce the formation of short-range order in the ACC, reducing the number of assessable conformations required until the perfect crystal structure is obtained. Finally, the additives may simply provide potential sites for nucleation.[55]

Considering in turn the low-molecular-weight additives, it is also possible that they could induce local ordering of the ACC, and maybe even provide nucleation sites. While short-range order resembling vaterite has been identified in PAsp-ACC using EXAFS, the same technique suggests that Mg-ACC may have short-range structures most similar to aragonite.[28] Indeed, a range of studies using techniques including NMR[56] and EXAFS[57,58] have indicated that ACC can exhibit different short-range orders according to the presence of occluded additives, and the precipitation conditions. Looking at the particular species investigated using DSC, magnesium ions had the greatest effect on the crystallization temperature and activation energy under the conditions used, increasing both as compared with the control calcite. This will, in part, derive from the higher hydration energy of Mg^{2+} as compared with Ca^{2+}, as the water must necessarily be lost before crystallization can occur.[15] As an additional effect, the product Mg-calcite is also thermodynamically less stable than pure calcite.[34,42] Sulfate ions again retarded the crystallization, where the reduction in thermodynamic stability of calcite on incorporation of sulfate is again likely to be a significant factor.[59] We would like to stress again, however, that care must be taken in making direct comparisons of the magnitude of the effects of the different additives, as this will necessarily depend on the concentrations of the additives employed, and, for example, on the density of functional groups in a polymer molecule. It is also clearly impossible to judge an equivalent concentration of ions (such as Mg^{2+}) and polymer additives.

Due to the experimental difficulties in studying nucleation processes, it is impossible to determine the origin of the additive-directed control over ACC crystallization conclusively in the current study. However, if nucleation of the product crystalline phases is indeed homogeneous, occurring within ACC particles, the influence of the additives on nucleation would be expected to be identical in the solid state and solution. Therefore, that a different pattern of behavior was observed in the solid state as compared with solution for the larger additives (PAsp, AOT, and PSS) demonstrates that the additives must also significantly affect the growth of the new crystalline phase. We suggest that additives are released from ACC particles into solution during their dissolution, which inhibits the growth of the new crystalline phase. A lesser effect would be expected in the solid state, where the additives are not free to move.

It is also interesting to consider biological calcification via an ACC precursor phase in light of these results. In the most-characterized system, that of sea urchin larvae, crystallization of ACC effectively occurs in the solid state. The ACC phase is located within a vesicle, where the initial hydrated ACC phases first dehydrates to give an anhydrous ACC phase, and crystallization then occurs via secondary nucleation.[8,20,21] No evidence for bulk water or dissolution of the ACC phase has been found. What then is the role of the macromolecules associated with this mineral phase? The experiments performed to-date have all examined the effects of organic molecules extracted from biogenic ACC phase on the crystallization of ACC in solution. In contrast, our results show that this does not necessarily provide a good test for their behavior in the solid state, where they can actually promote crystallization, depending on their size. Notably, however, biogenic ACC also typically contains magnesium ions, which significantly inhibit crystallization of ACC both in solution and in the solid state. It is therefore possible that combination of organic macromolecules and magnesium ions may enable organisms to tailor the stability of the amorphous calcium carbonate phase, which would allow control over its lifetime, and crystallization pathway; indeed, this would appear to be a key requirement in the use of ACC in biomineral formation. Carboxyl-rich biomolecules have also been shown to be able to regulate the Mg-content of magnesian calcite.[60] The organic additives could clearly also serve additional purposes, where retention within the crystal product can lead to a modification of the crystal texture and lead to enhanced mechanical properties.

4. Conclusions

In summary, our experimental results show for the first time that some additives can show a Janus like behavior, where they inhibit crystallization of amorphous calcium carbonate solution, while promoting it in the solid state. This effect was observed for all of the larger molecules examined in this study (poly(aspartic acid), poly(styrene sulfonate), and AOT), while the small molecules (magnesium and sulfate ions) retarded crystallization in both solution and the solid state. This provides insight into the mechanisms by which additives stabilize ACC against crystallization, such that in solution the overall effect is dominated by an inhibition of the growth of the crystalline phase due to additives released into the solution as the ACC phase dissolves. The dissolution of the ACC itself is little affected by the composition of the ACC, and the stability of ACC in solution is better considered as an indirect action of the additives on the new crystal phase rather than a direct effect on the structure/stability of the ACC itself. In contrast, the dominant effect of additives on the solid-state transformation of ACC appears to be on the nucleation of the new phase. Indeed, this would be consistent with suggestions that the incipient short-range structure of ACC can determine the structure of its crystalline transformation

product, both in synthetic and biogenic systems.[56,58] Finally, this work emphasizes that additives can play multiple roles in controlling crystallization processes, and it would be interesting to investigate the phenomena described here further, looking at a wider range of individual, and indeed combinations of additives.

5. Experimental Section

Materials: Analytical-grade sodium bis(2-ethylhexyl)sulfosuccinate (AOT) was purchased from Aldrich, and purified using standard literature methods.[61] Reference nanocalcite (≈100 nm in diameter) was obtained from American Elements. Magnesium chloride hexahydrate, anhydrous sodium carbonate, calcium chloride dihydrate, ammonium carbonate, poly(sodium 4-styrenesulfonate) (molecular weight (M.W.) = 70 000 g mol^{-1}), L-aspartic acid, and poly(α,β)-DL-aspartic acid sodium salt (M.W. = 2000–11 000 g mol^{-1}) were purchased in analytical grade from Sigma–Aldrich and used without further purification. 99.9% sodium hydroxide and 99% anhydrous sodium sulfate were obtained from Fischer Scientific. Solutions were prepared using Milli-Q water (18.2 MΩ cm^{-1}).

ACC Synthesis: ACC was synthesized using a number of methods. The majority of analyses were carried out using ACC which had been synthesized by mixing equal volumes of solutions of 1 M Na_2CO_3/30 mM NaOH (pH 12) and 1 M $CaCl_2$ (pH ≈ 6.8) at 4 °C. ACC formation occurred immediately after mixing both solutions and the precipitate was immediately filtered through a 0.22 µm Isopore GTTP membrane filter (Millipore), prior to washing with ethanol, and drying in a desiccator containing silica gel for 60 min. When required, selected additives were added either to the calcium chloride or carbonate solutions, prior to their mixing.

For comparison of ACC prepared by the different synthetic methods, ACC was also synthesized using a direct precipitation method (Direct ACC),[53] and the ammonia diffusion method.[9] "Direct ACC" was prepared by combining equal volumes of 1 M $NaCO_3$ (pH 11.8) with 1 M $CaCl_2$ (pH ≈ 6.8) at 4 °C. Immediate precipitation was observed at an apparent pH of ≈8.2 and the pH subsequently decreased to a final value of 6.8–7. The precipitate was immediately filtered through a 0.22 µm Isopore GTTP membrane filter (Millipore), prior to washing with ethanol, and drying in a desiccator containing silica gel for 60 min. In the ammonia diffusion method, a 10 mM solution of $CaCl_2$ was placed uncovered in a dish, which was then added to a hermetically closed container previously loaded with 3 g of ammonium carbonate. By this method, the initial neutral pH was raised to the pH 9, and remained over 9 throughout the entire reaction. Precipitate aliquots were removed from $CaCl_2$ solution at appropriate times to obtain specific polymorphs.

The ionic strength was calculated using Visual MinteQ for "Direct ACC" in the absence of additives, giving a value of $I = 1.217$. Only minor differences in this value occurred on addition of additives (200 ppm PAsp, -Asp, -AOT, -PSS, 10 mM Mg^{2+}, or 2 mM SO_4^{2-}) or 30 mM NaOH, giving values of $I = 1.218$ or $I = 1.224$ respectively. A significant change in ionic strength did occur on addition of 200 mM Mg^{2+} or SO_4^{2-}, but reference experiments in which NaCl was added to the initial solutions to achieve identical ionic strengths showed no difference in the observed trends (Supporting Information, Figure S9), indicating that this was not important in determining the pattern of results obtained.

Characterization: The $CaCO_3$ precipitates were characterized using Raman microscopy and IR spectroscopy, powder XRD, atomic absorption spectroscopy (AAS), thermogravimetric analysis (TGA) and modulated differential scanning calorimetry (MDSC), scanning electron microscopy (SEM), and transmission electron microscopy (TEM). Crystal morphologies were characterized using SEM by mounting glass slides supporting the $CaCO_3$ particles on SEM stubs using adhesive conducting pads and coating with Pt/Pd. Imaging was performed using a LEO 1530 Gemini FEG-SEM operating at 3 kV using an in-lens detector mode. TEM was carried out using a FEI Tecnai TF20 FEGTEM fitted with an HAADF detector and a Gatan Orius SC600A charge-coupled-deivce (CCD) camera, operating at 200 kV.

Individual crystal polymorphs were confirmed by Raman microscopy, using a Renishaw Raman 2000 System Microscope operating with a 785 nm laser, and by IR spectroscopy using a Perkin–Elmer ATR-IR instrument. The polymorphs and the polymorphic transition were further determined by powder XRD using a Bruker D8 Advanced diffractometer equipped with an X-ray source emitting Cu $K_{\alpha 1}$ radiation. Samples were placed on a piece of silicon wafer, and XRD data were collected in an angular range between 5° and 70° in intervals of 0.02°, with a scan rate of 1° min^{-1}. Polymorphic transitions were also followed by modulated DSC (TA Instruments DSC Q200), operating at heating rates of 5–25 °C min^{-1}, and a nitrogen flow rate of 100 mL min^{-1}. The compositions of the different ACC samples were investigated using TGA, where data were recorded using a TA Instruments STD Q600, operating at heating rates between 5 and 25 °C min^{-1} and 100 mL min^{-1} N_2 flow. The $CaCO_3$ samples containing Mg were additionally characterized by atomic absorption, where the precipitates were dissolved in 5% nitric acid and analyzed using a Perkin–Elmer atomic absorption spectrometer, AAnalyst 400 with an air-acetylene flame.

X-ray Absorption Spectroscopy (XAS) was carried out at the Ca-edge to investigate the short-range structure of the range of ACC samples, and data were collected on beamline B18 at the Diamond Synchrotron Source. Freshly prepared ACC samples were ground into a fine powder with boron nitride before being pressed into disks and were analyzed in transmission mode.

Investigation of ACC Crystallization in Solution: The influence of additives on the crystallization of ACC in solution was investigated using turbidity measurements to estimate the crystallization onset time of the different ACC samples, and by determining their dissolution profiles from conductivity measurements. Turbidity measurements were carried out as described previously.[29] Briefly, $CaCO_3$ was precipitated from solution by mixing 0.5 mL of 1 M $CaCl_2{\cdot}2H_2O$ with 0.5 mL 1 M Na_2CO_3 at 4 °C directly in spectrophotometer cuvettes, to give final solution concentrations of 0.5 M. When required, selected additives were added either to the calcium chloride or carbonate solutions with a final additive concentration of 100 ppm (Asp, PAsp, AOT, PSS) or 100 mM (Mg, SO_4). Measurements were performed using a Perkin–Elmer Lambda 35 system, operating in time-drive mode ($\lambda = 500$ nm, exposure time = 1 s).

The dissolution behavior of ACC, which had been precipitated in the absence and in the presence of additives, was investigated below the calcite solubility limit of <5.73 mg L^{-1}, at 25 °C.[62] Maintenance of this concentration ensured that no re-precipitation of the crystalline polymorphs of $CaCO_3$ could occur during dissolution of the ACC. Dissolution experiments were based on a modification of the procedure given by Meiron et al.,[63] where 1 mg of dried ACC was added to a closed Schott bottle filled with 250 mL of deionized water and equipped with a conductivity probe. The solution was kept under constant agitation (100 rpm). The dissolution progress was then tracked using time-resolved conductivity measurements, which allowed a selective investigation of the direct stabilization of ACC by additives incorporated within, or bound to the surface of the ACC particles. Solution conductivity measurements were performed using an InLab 731 Conductivity electrode (Metler Toledo).

Investigations of ACC Crystallization in the Solid State: Solid-state crystallization was studied by annealing samples, through thermogravimetric analysis (TGA) and DSC, and by performing in situ powder XRD analysis while heating the ACC precipitates. Studies of the phase transformation of dried ACC particles were carried out by simple heat treatment in a furnace, where the precipitates were heated at 10 °C min^{-1} to a maximum temperature of 70 °C, and were then incubated at this temperature for 12 h. TGA-DSC analyses were carried out using a TA-Instruments SDT Q600 Simultaneous TGA/DSC, with the measurements being performed under nitrogen in the temperature range from ambient to 400 °C with heating rates of 10 °C min^{-1}, 15 °C min^{-1}, and 20 °C min^{-1}. Identical amounts of sample (≈10 mg) were used in all of the runs. Powder XRD was also used to monitor crystallization of the ACC as a function of temperature in air. Samples were mounted on

glass slides and were heated in situ on the diffractometer. A heating rate of 5 °C min^{-1} was applied, and rapid scans were carried out over the interval $2\theta = 28–32$ degrees, to monitor the development of the (104) or (112) peaks of calcite and vaterite respectively. Characterization using IR spectroscopy and TEM before and after annealing the samples was also carried out to confirm polymorphs of the precipitates.

Supporting Information

Supporting Information is available from the Wiley Online Library or from the author.

Acknowledgements

We thank the EPSRC for financial support via grant number EP/H005374/1 (J.I., Y.Y.K., and F.C.M.). The authors would also like to thank Diamond for the provision of beam-time, and we are most grateful for the assistance of Dr. Giannantonio Cibin, on the B18 Core XAS beamline, for all his assistance in setting-up and collecting the XAS data. Thanks also to Diamond for financially supporting our stay, project reference number SP6114.

Received: July 2, 2012
Revised: September 7, 2012
Published online: October 19, 2012

[1] H. A. Lowenstam, S. Weiner, *On Biomineralization*, Oxford University Press, New York **1989**.
[2] F. C. Meldrum, H. Colfen, *Chem. Rev.* **2008**, *108*, 4332.
[3] J. Aizenberg, N. Ilan, S. Weiner, L. Addadi, *Connective Tissue Res.* **1996**, *35*, 17.
[4] A. M. Belcher, X. H. Wu, R. J. Christensen, P. K. Hansma, G. D. Stucky, D. E. Morse, *Nature* **1996**, *381*, 56.
[5] B. A. Gotliv, L. Addadi, S. Weiner, *ChemBioChem* **2003**, *4*, 522.
[6] S. Weiner, L. Addadi, *Annu. Rev. Mater. Res.* **2011**, *41*, 21.
[7] L. B. Gower, *Chem. Rev.* **2008**, *108*, 4551.
[8] Y. U. T. Gong, C. E. Killian, I. C. Olson, N. P. Appathurai, A. L. Amasino, M. C. Martin, L. J. Holt, F. H. Wilt, P. U. P. A. Gilbert, *Proc. Natl. Aacd. Sci. USA* **2012**, *109*, 3699.
[9] J. Aizenberg, G. Lambert, S. Weiner, L. Addadi, *J. Am. Chem. Soc.* **2002**, *124*, 32.
[10] A. Sato, S. Nagasaka, K. Furihata, S. Nagata, I. Arai, K. Saruwatari, T. Kogure, S. Sakuda, H. Nagasawa, *Nat. Chem. Biol.* **2011**, *7*, 197.
[11] X. R. Xu, A. H. Cai, R. Liu, H. H. Pan, R. K. Tang, K. W. Cho, *J. Cryst. Growth* **2008**, *310*, 3779.
[12] B. Guillemet, M. Faatz, F. Grohn, G. Wegner, Y. Gnanou, *Langmuir* **2006**, *22*, 1875.
[13] L. B. Gower, D. J. Odom, *J. Cryst. Growth* **2000**, *210*, 719.
[14] J. Jiang, M. R. Gao, Y. H. Qiu, S. H. Yu, *Nanoscale* **2010**, *2*, 2358.
[15] E. Loste, R. M. Wilson, R. Seshadri, F. C. Meldrum, *J. Cryst. Growth* **2003**, *254*, 206.
[16] K. Sawada, *Pure Appl. Chem.* **1997**, *69*, 921.
[17] B. Cantaert, Y. Y. Kim, H. Ludwig, F. Nudelman, N. Sommerdijk, F. C. Meldrum, *Adv. Funct. Mater.* **2012**, *22*, 907.
[18] S. E. Wolf, J. Leiterer, V. Pipich, R. Barrea, F. Emrnerling, W. Tremel, *J. Am. Chem. Soc.* **2011**, *133*, 12642.
[19] A. Gal, S. Weiner, L. Addadi, *J. Am. Chem. Soc.* **2010**, *132*, 13208.
[20] E. Beniash, L. Addadi, S. Weiner, *J. Struct. Biol.* **1999**, *125*, 50.
[21] Y. Politi, R. A. Metzler, M. Abrecht, B. Gilbert, F. H. Wilt, I. Sagi, L. Addadi, S. Weiner, P. Gilbert, *Proc. Natl. Aacd. Sci. USA* **2008**, *105*, 17362.
[22] Y. Y. Kim, N. B. J. Hetherington, E. H. Noel, R. Kroger, J. M. Charnock, H. K. Christenson, F. C. Meldrum, *Angew. Chem. Int. Ed.* **2012**, *50*, 12572.
[23] C. J. Stephens, S. F. Ladden, F. C. Meldrum, H. K. Christenson, *Adv. Funct. Mater.* **2010**, *20*, 2108.
[24] M. Kellermeier, E. Melero-Garcia, F. Glaab, R. Klein, M. Drechsler, R. Rachel, J. M. Garcia-Ruiz, W. Kunz, *J. Am. Chem. Soc.* **2010**, *132*, 17859.
[25] H. S. Lee, T. H. Ha, K. Kim, *Mater. Chem. Phys.* **2005**, *93*, 376.
[26] N. V. Vagenas, A. Gatsouli, C. G. Kontoyannis, *Talanta* **2003**, *59*, 831.
[27] M. M. Tlili, M. B. Amor, C. Gabrielli, S. Joiret, G. Maurin, P. Rousseau, *J. Raman Spectrosc.* **2002**, *33*, 10.
[28] R. S. K. Lam, J. M. Charnock, A. Lennie, F. C. Meldrum, *CrystEngComm* **2007** *9*, 1226.
[29] Y. W. Wang, Y. Y. Kim, C. J. Stephens, F. C. Meldrum, H. K. Christenson, *Cryst. Growth Des.* **2012**, *12*, 1212.
[30] C. J. Stephens, Y. Y. Kim, S. D. Evans, F. C. Meldrum, H. K. Christenson, *J. Am. Chem. Soc.* **2011**, *133*, 5210.
[31] T. Y. J. Han, J. Aizenberg, *Chem. Mater.* **2008**, *20*, 1064.
[32] J. R. I. Lee, T. Y. J. Han, T. M. Willey, D. Wang, R. W. Meulenberg, J. Nilsson, P. M. Dove, L. J. Terminello, T. van Buuren, J. J. De Yoreo, *J. Am. Chem. Soc.* **2007**, *129*, 10370.
[33] D. Pontoni, J. Bolze, N. Dingenouts, T. Narayanan, M. Ballauff, *J. Phys. Chem. B* **2003**, *107*, 5123.
[34] J. W. Morse, R. S. Arvidson, A. Luttge, *Chem. Rev.* **2007**, *107*, 342.
[35] A. V. Radha, T. Z. Forbes, C. E. Killian, P. U. P. A. Gilbert, A. Navrotsky, *Proc. Natl. Aacd. Sci. USA* **2010**, *107*, 16438.
[36] N. Koga, Y. Nakagoe, H. Tanaka, *Thermochim. Acta* **1998**, *318*, 239.
[37] N. Koga, Y. Yamane, T. Kimura, *Thermochim. Acta* **2011**, *512*, 13.
[38] X. Xu, J. T. Han, D. H. Kim, K. Cho, *J. Phys. Chem. B* **2006**, *110*, 2764.
[39] M. Avrami, *J. Chem. Phys.* **1940**, *8*, 212.
[40] T. Ozawa, *J. Therm. Anal. Cal.* **1970**, *2*, 301.
[41] M. M. Reddy, G. H. Nancollas, *J. Cryst. Growth* **1976**, *35*, 33.
[42] K. J. Davis, P. M. Dove, J. J. De Yoreo, *Science* **2000**, *290*, 1134.
[43] H. J. Meyer, *J. Cryst. Growth* **1984**, *66*, 639.
[44] L. J. Plant, W. A. House, *Colloids Surf. A* **2002**, *203*, 143.
[45] C. A. Orme, A. Noy, A. Wierzbicki, M. T. McBride, M. Grantham, H. H. Teng, P. M. Dove, J. J. DeYoreo, *Nature* **2001**, *411*, 775.
[46] S. Elhadj, E. A. Salter, A. Wierzbicki, J. J. De Yoreo, N. Han, P. M. Dove, *Cryst. Growth Des.* **2006**, *6*, 197.
[47] A. I. Vavouraki, C. V. Putnis, A. Putnis, P. G. Koutsoukos, *Chem. Geol.* **2008**, *253*, 243.
[48] J. Kontrec, D. Kralj, L. Brecevic, G. Falini, S. Fermani, V. Noethig-Laslo, K. Mirosavljevic, *Eur. J. Inorg. Chem.* **2004**, 4579.
[49] J. J. De Yoreo, A. Wierzbicki, P. M. Dove, *CrystEngComm* **2007**, *9*, 1144.
[50] E. M. Pouget, P. H. H. Bomans, J. Goos, P. M. Frederik, G. de With, N. Sommerdijk, *Science* **2009**, *323*, 1455.
[51] F. Nudelman, E. Sonmezler, P. H. H. Bomans, G. de With, N. A. J. M. Sommerdijk, *Nanoscale* **2010**, *2*, 2436.
[52] C. C. Tester, R. E. Brock, C. H. Wu, M. R. Krejci, S. Weigand, D. Joester, *CrystEngComm* **2011**, *13*, 3975.
[53] J. D. Rodriguez-Blanco, S. Shaw, L. G. Benning, *Nanoscale* **2011**, *3*, 265.
[54] D. Zhou, G. G. Z. Zhang, D. Law, D. J. W. Grant, E. A. Schmitt, *J. Pharm. Sci.* **2002**, *91*, 1863.
[55] C. Bhugra, M. J. Pikal, *J. Pharm. Sci.* **2008**, *97*, 1329.
[56] D. Gebauer, P. N. Gunawidjaja, J. Y. P. Ko, Z. Bacsik, B. Aziz, L. J. Liu, Y. F. Hu, L. Bergstrom, C. W. Tai, T. K. Sham, M. Eden, N. Hedin, *Angew. Chem. Int. Ed.* **2011**, *49*, 8889.
[57] Y. Politi, Y. Levi-Kalisman, S. Raz, F. Wilt, L. Addadi, S. Weiner, I. Sagi, *Adv. Funct. Mater.* **2006**, *16*, 1289.

[58] B. Hasse, H. Ehrenberg, J. C. Marxen, W. Becker, M. Epple, *Chem. Eur. J.* **2000**, *6*, 3679.
[59] E. Busenberg, L. N. Plummer, *Geochim. Cosmochim. Acta* **1985**, *49*, 713.
[60] D. B. Wang, A. F. Wallace, J. J. De Yoreo, P. M. Dove, *Proc. Natl. Aacd. Sci. USA* **2009**, *106*, 21511.
[61] E. Y. Sheu, S. H. Chen, *J. Phys. Chem.* **1988**, *92*, 4466.
[62] L. N. Plummer, E. Busenberg, *Geochim. Cosmochim. Acta* **1982**, *46*, 1011.
[63] O. E. Meiron, E. Bar-David, E. D. Aflalo, A. Shechter, D. Stepensky, A. Berman, A. Sagi, *J. Bone Miner. Res.* **2011**, *26*, 364.